PHYSICAL REVIEW B **81**, 104105 (2010)

Dielectric and soft-mode behaviors of $AgTaO_3$

Hwee Ping Soon, Hiroki Taniguchi, and Mitsuru Itoh[*]
Materials and Structure Laboratory, Tokyo Institute of Technology, Yokohama 226-8503, Japan

(Received 18 August 2009; published 12 March 2010)

The synthesis difficulty on $AgTaO_3$ ceramic has been surmounted by the high oxygen-pressure sintering. In this study, the synthesized sample was investigated by both dielectric and micro-Raman measurements in detail. As no dielectric anomaly was observed between 2.2 and 694 K, the previously proposed ferroelectric phase transition from $R3c$ to $R\bar{3}c$ at 170 K upon heating is not supported by our study whereas the quantum paraelectric ground state with $R\bar{3}c$ symmetry is more consistent with our experimental findings. Also, it is observed that the phase transition from this rhombohedral ground state to the higher-temperature monoclinic phase occurs at 667 K is purely soft-mode driven. Taking account the observation of additional Raman modes, at least up to 360 K, the existence of symmetry-breaking regions in the quantum paraelectric matrix is also discussed.

DOI: 10.1103/PhysRevB.81.104105 PACS number(s): 77.84.−s, 63.20.−e, 78.30.−j

I. INTRODUCTION

Despite of the numerous explorations of perovskite-type materials, the classical silver-based ABO_3 perovskite-type niobates and tantalates that exhibit distorted pseudocubic structures have been surprisingly left aside. Until recently, silver-based perovskite oxides have started to gain surged interests due to the discoveries of their ultralow dielectric losses and photocatalytic properties that meet the requirements of the demanding telecommunication and solar-energy applications.[1,2] Also, our research group has discovered the large polarization and electromechanical responses of $AgNbO_3$ (Ref. 3). Although the silver-based perovskites have shown various attractive physical properties, the difficulties encountered in synthesis resulted from the thermal instability of Ag^+ ion at elevated temperatures has hindered the explorations of this class of materials.[2] In particular, the synthesis of $AgTaO_3$ (AT) and AT-rich solid solutions serves as the greatest challenge among all the silver-based perovskites owing to the requirement of high sintering temperature, which is usually higher than the decomposition temperature. Although the recent development of wet-chemistry and low-temperature sintering methods have surpassed the synthesis difficulties of AT-rich solid solutions,[4,5] these processing routes are either complicated or involve the usage of impurities for decreasing the sintering temperature. Also, the synthesis difficulty of pure AT ceramics still remains unsolved.

In addition to the limited explorations due to the synthesis difficulty, the phase-transition sequence of AT also remains unsettled. At the present stage, it is generally agreed that AT undergoes a series of phase transitions from rhombohedral ($T \leq 685$ K) to monoclinic ($650\text{ K} \leq T \leq 703$ K) and then to tetragonal ($685\text{ K} < T \leq 780$ K), and finally to cubic at $T_{\text{T-C}} = 780$ K upon heating, as suggested by x-ray diffraction (XRD) measurements, differential thermal analyses (DTA) and Raman investigations on AT single crystal. The temperatures given in the parenthesis indicate the temperature range for the existence of each phase.[6,7] However, due to the coexistences regions between rhombohedral and monoclinic ($650\text{ K} \leq T \leq 685$ K), and monoclinic and tetragonal ($685\text{ K} < T \leq 703$ K), the actual transition temperatures from rhombohedral to monoclinic $T_{\text{R-M}}$ as well as that from monoclinic to tetragonal $T_{\text{M-T}}$ still remain uncertain. Kugel *et al.*[6] selected $T_{\text{R-M}} = 667$ K and $T_{\text{M-T}} = 694$ K, where these temperatures correspond to the centers of temperature ranges of the aforementioned phase-coexistence regimes. Furthermore, the origins that trigger these phase transitions still remain unclear.

In addition to the aforementioned phase transitions, it has also been argued that an additional phase transition from a ferroelectric rhombohedral phase with $R3c$ symmetry (Glazer notation:[8] $a^-a^-a^-$ and displacement) to the paraelectric rhombohedral phase with $R\bar{3}c$ symmetry ($a^-a^-a^-$) occurs at 170 K upon heating due to the observation of additional Raman modes and weak pyroelectricity with spontaneous polarization (P_s) deduced as $0.02\ \mu\text{C/cm}^2$ at 80 K.[6] Komandin *et al.*[9] further proposed that AT is possibly an improper ferroelectric by considering the absence of soft-mode anomaly for this phase transition. In contrast, Wołcyrz and Łukaszewski[10] reported that AT is more likely a ferroelectric phase with $R3c$ symmetry at room temperature (RT) on the basis of the detailed analyses of weaker reflections and Halmilton test, although the small difference in reliability factor for their refinement to both $R3c$ and $R\bar{3}c$ symmetries could not lead to a conclusive decision. This eventually opposes the aforementioned argument on the existence of paraelectric phase with $R\bar{3}c$ symmetry and the corresponding phase transition. On the basis of these controversial research works, one can conjecture that AT exhibits a ferroelectric phase transition from the ground-state rhombohedral structure with $R3c$ symmetry to either (1) the paraelectric monoclinic phase at $\sim T_{\text{R-M}}$ or to (2) the paraelectric rhombohedral phase with $R\bar{3}c$ symmetry at 170 K upon heating. With this physical picture, a dielectric anomaly is then expected due to the change in order parameter, namely, P_s, upon the ferroelectric phase transition from $R3c$ ($P_s \neq 0$) to either of the possible paraelectric phases ($P_s = 0$) based on the Landau theory; however, it is observed that $\varepsilon'(T)$ decreases monotonically from ~ 50 K,[5] which is the lowest temperature for the available dielectric measurement up to now. Although Kugel *et al.*[6] claimed that a subtle anomaly was observed in their dielectric measurement as well as the temperature dependence of lattice parameter at ∼120 K upon heating, this temperature is much lower than that suggested by their Raman and pyroelectric measurements at 170 K. Also, there occurred similar or even more obvious anomalies at many other temperatures at which a phase transition was not expected in their dielectric measurement, indicating that the attribution of subtle anomaly at 120 K to the dielectric anomaly brought about by the ferroelectric phase transition from $R3c$ to $R\bar{3}c$ symmetry is rather uncertain. By consolidating all the reported data, the present physical picture for AT is indeed controversial and requires further clarification, particularly in the following two aspects: (1) the existence of phase transition from ferroelectric $R3c$ ground state to higher-temperature phase with $R\bar{3}c$ symmetry at 170 K and (2) the unknown origin of phase transition from the rhombohedral ground state to the higher-temperature monoclinic phase.

In this study, we first surmounted the long-standing synthesis difficulty of AT by a simple processing route involving only the conventional solid-state reaction and sintering in environment with a high oxygen pressure at ∼13 atm. This methodology led to a high-quality polycrystalline AT, by which the flux, i.e., V_2O_3, that may serve as the source of contamination required for crystal growth can be eliminated. The XRD traces that confirm the phase formation of AT are given in Sec. III A. Following the synthesis of AT polycrystalline sample, we revisit the controversial physical picture for AT rhombohedral phase and its subsequent phase transition by performing both dielectric and micro-Raman measurements in detail down to 2.2 and 3.5 K, respectively. The absence of dielectric anomaly indicates that the ferroelectric phase transition from $R3c$ to $R\bar{3}c$ symmetry is very unlikely, as detailed in Sec. III A. Also, our micro-Raman measurements show that the phase transition from rhombohedral to the subsequent monoclinic phase upon heating is soft-mode driven. The mode assignments as well as the spectra analyses are given in Secs. III B and III C, respectively.

II. EXPERIMENTAL DETAILS

In our synthesizing route, the constituent oxide, Ag_2O and Ta_2O_5, first undergo a grind mixing and calcined at 1000 °C for 6 h. The calcined powder was then pressed into a pellet in 6 mm in diameter. Sintering was carried out by placing the powder compact into a sealed zirconia tube that was connected to a pressure control valve. Prior to the sintering, oxygen gas at ∼6.25 atm was filled into the sealed zirconia tube after the evacuation. Upon heating, the pressure of sealed oxygen gas increased and reached ∼13 atm when the powder compact was sintered at 1300 °C for 2 h. This eventually led to formation of dense polycrystalline AT. The formation of rhombohedral single-phase AT was confirmed by the XRD measurements. Also, the lattice parameters for AT were computed by the XRD traces obtained at $70° \leq 2\theta \leq 120°$ with Si powder added as an internal standard. The dielectric measurements were performed by employing HP4284A LCR meter with an ac electric field of 1 V/mm at temperature ranging from 2.2 to 820 K. The confocal micro-Raman measurements were performed by the Jobin-Yvon T64000 with triple monochromator micro-Raman system with the aids of a high objective lens (NA=0.5) and a 514.5 nm Ar^+ green laser (∼10 mW). The ambient temperature of the sample was precisely controlled by employing the Oxford Microstat with a temperature stability of ±0.02 K for $3.5\ \text{K} \leq T < 400\ \text{K}$ and the Linkam TS1500 heating stage with temperature stability of ±1 °C for $T \geq 400$ K.

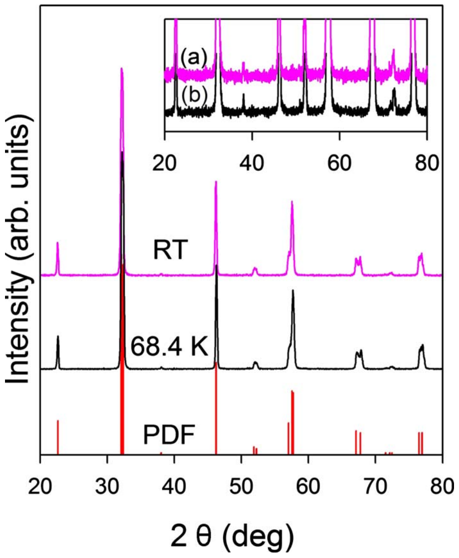

FIG. 1. (Color online) XRD traces for AT obtained at RT and 68.4 K together with the standard pattern given by the powder diffraction file No. 01-072-1383. The inset further enlarges the XRD traces for (a) RT and (b) 68.4 K, respectively.

III. RESULTS

A. Phase formation and dielectric measurements

Figure 1 plots the XRD traces of synthesized AT obtained at RT, 68.4 K and the standard pattern given by the powder diffraction file (No. 01-072-1383), respectively. The close agreement between the experimental data and the standard pattern indicates the formation of single-phase AT. Furthermore, the computed lattice parameter a_R and interaxial angle α of AT rhombohedral cell at RT are 5.5758 Å and 59.4458°, respectively, which is consistent with the reported values for AT single crystal with $R\bar{3}c$ symmetry.[10] The average crystallite size t estimated using the Scherrer's equation, $t = 0.9\lambda / B \cos\theta$, is ∼36 nm, where λ, B, and θ denote the x-ray wavelength (Cu $K\alpha = 1.54060$ Å), full width half maximum of a diffraction peak and the corresponding Bragg's angle, respectively. Upon cooling the sample to 68.4 K, neither additional peak nor significant change in intensity was observed, indicating that the same rhombohedral phase persists down to low temperatures.

The temperature dependence of ε' and $1/\varepsilon'$ for AT measured at 1 MHz upon heating are depicted in Fig. 2. $\varepsilon'(T)$ obtained at lower frequencies varies subtly from that of 1 MHz. As shown in Fig. 2 and the inset, two steplike dielec-

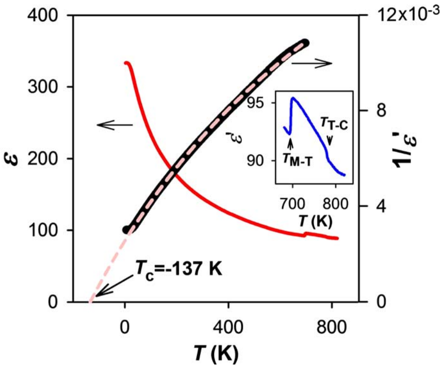

FIG. 2. (Color online) Temperature dependences of ε' and $1/\varepsilon'$ fitted to the Curie-Weiss law (dashed line) for AT measured at 1 MHz upon heating. The inset further shows the steplike phase transitions from monoclinic to tetragonal and then to cubic at $T_{\text{M-T}}=694$ K and $T_{\text{T-C}}=780$ K, respectively.

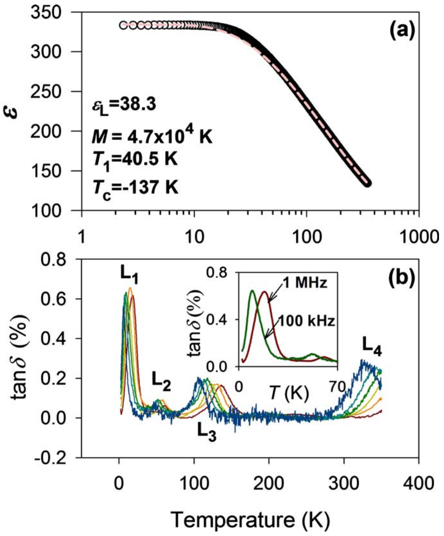

FIG. 3. (Color online) Temperature dependence of ε' together with the fitting to the Barrett's relation indicated by the dashed line (a) tan δ measured at frequency ranging from 20 kHz to 1 MHz and (b) for AT.

tric anomalies corresponding to the phase transitions from monoclinic to tetragonal and tetragonal to cubic were observed at 694 and 780 K, respectively. This observation is in agreement with the previous reports.[6,7] Below 694 K, ε' increases smoothly and levels off at sufficiently low temperatures, whereby no anomaly was observed in ε'. Furthermore, the temperature dependence of $1/\varepsilon'$ for AT shows nonlinear behavior, which is similar to that of KTaO$_3$, obeying the modified form of the Curie-Weiss law[11,12]

$$\varepsilon' = \varepsilon_{\text{L}} + \frac{C}{T - T_{\text{c}}}, \tag{1}$$

where C and T_{c} are the Curie-Weiss constant and phase-transition temperature, respectively. The constant ε_{L} shows the temperature independent term of ε', which is the summation of the contributions to ε' by the electronic polarizability on the order of 5–6, the optical lattice modes with frequencies change subtly with temperature and the soft optical lattice mode at $T \to \infty$.[12] In order to determine T_{c} with a good accuracy, a strong weighting was adjusted for the experimental data obtained at $500 \text{ K} < T \leq 600$ K when performing the fitting. The best fitting to the modified Curie-Weiss law for AT gives $\varepsilon_{\text{L}}=38.2$, $C=4.7\times10^4$ K, and $T_{\text{c}}=-137$ K, respectively. As shown in Fig. 3(a), the temperature dependence of ε' is further fitted to the Barrett's relation that characterizes the quantum paraelectricity[13]

$$\varepsilon' = \varepsilon_{\text{L}} + \frac{M}{(T/2)\coth(T_1/2T) - T_{\text{c}}}, \tag{2}$$

where M and T_1 denote the Curie-Weiss constant and the saturation temperature, respectively. $T_{\text{c}}=-137$ K determined by the fitting to Eq. (1) in a good accuracy was employed during the fitting to Eq. (2). The quality of the fitting is similar to those obtained for the quantum paraelectric SrTiO$_3$ (Ref. 14) and La$_{0.5}$Na$_{0.5}$TiO$_3$ (Ref. 15), whereby slight deviation was observed at the intermediate temperature range $13 \text{ K} < T < 60$ K, when T_1 was adjusted to fit the low-temperature regime. The best-fitted parameters are listed in Fig. 3(a). Figure 3(b) depicts the temperature dependence of tan δ obtained at frequency ranging from 20 kHz to 1 MHz. In general, the low tan δ indicates the good quality of the sample. In contrast to the plain profile observed in $\varepsilon'(T)$, four dielectric loss peaks denoted by L$_1$–L$_4$ were observed in the temperature dependence of tan δ, as shown in Fig. 3(b). It is observed that all L$_1$–L$_4$ shift to higher temperatures with increasing frequencies, indicating the occurrence of thermally activated relaxation processes that can be described by the Arrhenius law, $\omega=\omega_{\text{o}}\exp(-E/k_{\text{B}}T)$, as depicted in Figs. 4(a)–4(d) together with the best-fitted parameters. ω_{o}, E, and k_{B} in the Arrhenius law denote the attempt frequency, activation energy, and Boltzmann constant, respectively.

Next, we consolidate all the physical information suggested by the dielectric measurements. First, no dielectric

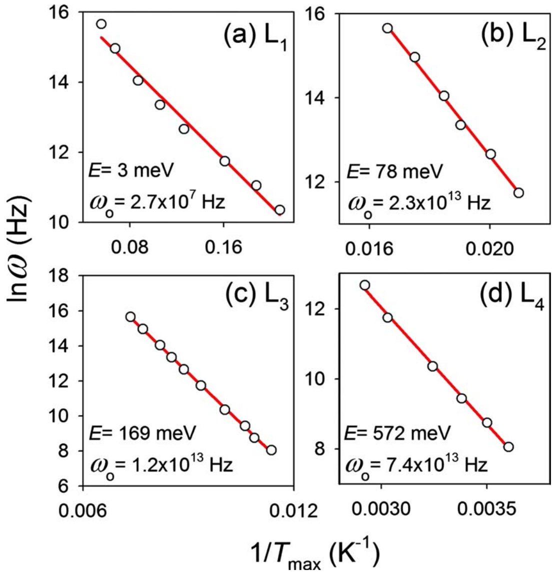

FIG. 4. (Color online) Arrhenius plots for the relaxation processes denoted by (a) L$_1$, (b) L$_2$, (c) L$_3$, and (d) L$_4$, respectively.

anomaly was observed at the two possible phase-transition temperatures proposed by the previous studies, namely, at $\sim T_{\text{R-M}}=667$ K (ferroelectric $R3c$ phase to paraelectric monoclinic) and 170 K (ferroelectric $R3c$ to paraelectric $R\bar{3}c$), as clearly shown in Fig. 2. As an induced P_s should trigger a dielectric anomaly, this indicates that the occurrence of ferroelectric phase transition from $R3c$ state to any of the high-temperature states is very unlikely. Second, the four tan δ peaks demonstrated in Fig. 3(b) are not related to the ferroelectric phase transition but would stem from merely the thermally activated relaxation processes probably due to the defects or impurities in the sample. Similar behavior was also observed in $SrTiO_3$.[16] This is indeed in agreement with the first argument. Third, the negative T_c given by both Barrett's and Curie-Weiss relations consistently suggested that phase transition should not occur at any attainable temperatures upon heating up to 600 K, which is consistent with the XRD traces shown in Fig. 1. By considering the rhombohedral phase confirmed by our XRD measurements and other literatures mentioned previously, our dielectric measurement supports that a paraelectric phase with an average structure of rhombohedral $R\bar{3}c$ symmetry should be the stable phase at least down to 2.2 K, whereby the ferroelectric phase transition is very unlikely. Furthermore, the level-off of ε' observed at sufficiently low temperatures could be brought about by the quantum mechanical fluctuations,[17] indicating the quantum paraelectricity of AT, as demonstrated by the Barrett's fitting in Fig. 3(a).

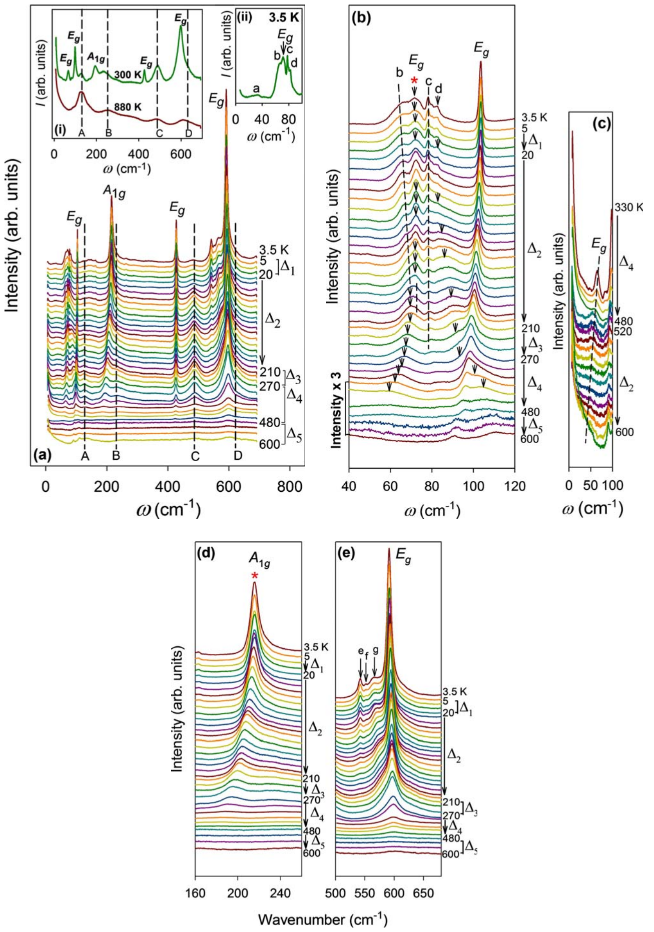

FIG. 5. (Color online) Temperature dependence of Raman spectra for AT obtained upon heating from 3.5 K with (a) the temperature intervals $\Delta_1=5$ K, $\Delta_2=10$ K, $\Delta_3=20$ K, $\Delta_4=30$ K, and $\Delta_5=50$ K. The insets in (a) further compare the spectra obtained at (i) RT and 880 K and plot the Raman spectra with (ii) wave number ranging from ~6 to 120 cm^{-1} obtained at 3.5 K, respectively. Enlargements of spectra in (a) at wave number ranging from 40 to 120 cm^{-1} (b), 160 to 250 cm^{-1} (d) and 500 to 680 cm^{-1} (e), respectively. Softening of E_g mode at temperature ranging from 330 to 600 K is further detailed in (c). The dashed lines and arrows show the eye guides.

B. Raman measurements: Mode assignments

In the previous section, the dielectric measurements have pointed out the unlikelihood for the occurrence of ferroelectric phase transition, which on the other hand suggests the phase transition from the rhombohedral paraelectric phase with $R\bar{3}c$ symmetry to the higher-temperature monoclinic phase. Therefore, we further explore such a transition by performing micro-Raman measurements.

The factor-group analysis of the optical lattice vibration for $R\bar{3}c$ symmetry gives the irreducible representation of normal modes as[18,19]

$$\Gamma_{\rm v} = A_{1g}(\mathrm{R}) + 2A_{1u} + 3A_{2g} + 3A_{2u}(\mathrm{IR}) + 4E_g(\mathrm{R}) + 5E_u(\mathrm{IR}),$$

where R and IR in the parenthesis denote the Raman-active and infrared-active modes, respectively. The five modes, namely, $4E_g+A_{1g}$, originate from the zone-boundary R-point of the Brillouin zone of high-temperature cubic phase become Raman active due to the cell doubling resulted by the alternating rotations (or tilts) of oxygen octahedra ($a^-a^-a^-$) about the [111] of cubic axis.[18,19] If the structure changes to $R3c$ symmetry ($a^-a^-a^-$+displacement), the Raman selection rules are relaxed due to the breaking of inversion center brought about by the additional displacement, leading to the activation of additional five E modes and three A_1 modes that are originally IR active for $R\bar{3}c$ symmetry.

Figure 5(a) depicts the Raman spectra for AT obtained at temperature ranging from 3.5 to 600 K upon heating. The inset (i) in Fig. 5(a) further compares the spectra obtained at both RT and 880 K. Clearly, bands A–D were observed for the spectrum obtained at 880 K for AT cubic phase, although the first-order Raman scattering is forbidden. It is also observed that the intensities of bands A–D increase with increasing temperature, as shown in Fig. 5(a). Therefore, they are attributed to the second-order scattering. In contrast, the spectrum obtained at 300 K consists of another five additional first-order modes together with bands A–D. The total number of additional modes is consistent with that suggested by the factor-group analysis for $R\bar{3}c$ symmetry ($4E_g+A_{1g}$), which further agrees with our RT XRD and also with other reports on the structural analyses for AT single crystal.[10] Furthermore, Figs. 5(b) and 5(d) show the details of Raman spectra at wave number ranging from 40 to 120 cm^{-1} and 160 to 250 cm^{-1}, respectively. Upon heating from 3.5 K, two softening modes were observed, as marked by the asterisks. The two softening modes can be attributed to the rota-

TABLE I. Comparison of Raman modes observed at 3.5 and 300 K. The asterisks indicate the softening modes.

Raman modes	ω (cm^{-1}) at 3.5 K	ω (cm^{-1}) at 300 K
a	32	44
b	65	
E_g^*	72	66
c	78	82
d	81	98
E_g	104	101
A_{1g}^*	216	193
E_g	428	426
e	542	
f	553	
g	566	
E_g	592	597

tional E_g and A_{1g} modes split from the Γ_{25}-phonon branch at the R point of Brillouin zone for cubic phase that results in $R\bar{3}c$ symmetry.[19] Since the frequency of A_{1g} mode is commonly higher than that of E_g mode in the perovskites, for example, in $LaAlO_3$ that also exhibits $R\bar{3}c$ symmetry, the softening modes at ~65 and ~185 cm^{-1} are assigned as E_g and A_{1g} modes, respectively. Also, it is observed that the soft E_g mode first crosses with mode b, as marked by the arrows and the dashed lines in Fig. 5(b), respectively, and then becomes a central peak (CP) like structure at 600 K, as shown clearly in Fig. 5(c). Having a close look at Fig. 5(b), the soft E_g mode seems to anticrosses with mode b with some intensity transference. In addition to the two softening modes, the other three hard modes observed in the RT spectrum can be further assigned as E_g modes on the basis of factor-group analysis ($4E_g+A_{1g}$). Following the assignments of E_g^1 mode at ~65 cm^{-1}, E_g^2 at ~100 cm^{-1}, E_g^3 at ~424 cm^{-1}, E_g^4 at ~596 cm^{-1} (the superscript is used to differentiate the four E_g modes with different frequencies) and A_{1g} at 185 cm^{-1}, the second-order scattering denoted by A–D at ~130, 253, 486, and 610 cm^{-1} can be resulted from $2E_g^1$ (overtone) and/or $A_{1g}-E_g^1$ (difference combination), $A_{1g}+E_g^1$ (additional combination), $E_g^3+E_g^1$ (additional combination) and $A_{1g}+E_g^3$ (additional combination), respectively.

In contrast to the spectra obtained at 300 K, additional modes denoted by a–g were observed at lower temperatures, as depicted in the inset (ii) of Figs. 5(a), 5(b), and 5(e). The frequencies of additional modes a–g at both 3.5 and 300 K are summarized in Table I. The activation of these additional modes was previously interpreted as the evidence for the phase transition from ferroelectric $R3c$ to paraelectric $R\bar{3}c$ symmetry by considering the activation of IR modes due to the breaking of inversion center and the weak pyroelectricity observed for AT.[6,9] This physical picture will again be addressed and further discussed later in this study.

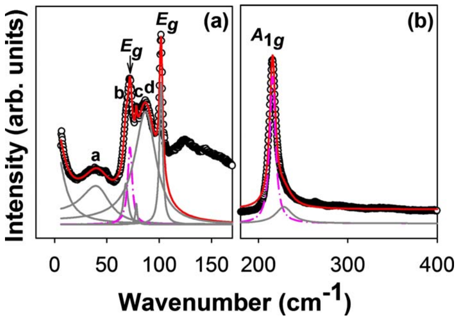

FIG. 6. (Color online) The fitting examples using the DHO model for the soft (a) E_g and (b) A_{1g} analyzes for the spectra obtained at 150 and 3.5 K, respectively. The dashed-dotted lines show the fittings for the soft modes.

C. Soft-mode-driven rhombohedral to monoclinic phase transition

To further quantify the temperature dependence of frequency for soft E_g and A_{1g} modes (ω_s), the Raman spectra ranging from ~6 to 104 cm^{-1} and ~150 to 400 cm^{-1} were analyzed by a damped-harmonic-oscillator (DHO) model. In this model, the intensity $I(\omega)$ of the spectra can be described by

$$I(\omega) \propto \begin{bmatrix} n(\omega)+1 \\ n(\omega) \end{bmatrix} \left[\frac{S_r \omega \tau}{1+(\omega\tau)^2} + \sum_i \frac{S_i \omega_i^2 \omega \Gamma_i}{(\omega_i^2-\omega^2)^2+(\omega\Gamma_i)^2} \right]. \tag{3}$$

The $n(\omega)$ term in the first bracket denotes the population factor while the two terms in the second bracket correspond to the CP and the summation of the contributions of soft and hard E_g modes and modes a–d, respectively. The fitted parameters S_r, τ, S_i, ω_i, and Γ_i denote the amplitude and relaxation time of CP, and amplitude, harmonic frequency, and the damping constant of vibrational mode i, respectively. In additional to the model mentioned above, it is also assumed that the spectrum with frequency >104 cm^{-1} has negligible influence on the low-frequency spectrum and masked from the fitting when analyzing the soft E_g mode. On the other hand, another three assumptions were also taken when analyzing the soft A_{1g} mode: (1) the spectra with wave number ranging from ~6 to the minimum observed at ~150 cm^{-1} as well as that with wave number >400 cm^{-1} were assumed to have negligible influence and masked from the fitting, thereby S_r in Eq. (3) that describes the CP was also set to zero; (2) the fitted spectrum consists of A_{1g} and the second-order scattering band B, which can be described by two DHOs; and (3) the spectrum ranging from 360 to 400 cm^{-1} that is rather featureless is employed as the background for the fitting. Due to the broad and overlapped spectra at T >360 K, the spectra analyses for A_{1g} were performed only up to 360 K. The fitting examples for the spectra obtained at 150 and 3.5 K employed for the soft E_g and A_{1g} modes analyses are demonstrated in Figs. 6(a) and 6(b), respectively. The ω_s for the soft E_g and A_{1g} modes is further computed by $\omega_s=[\omega_i^2-(\Gamma_i/2)^2]^{1/2}$, which corresponds to the frequency that coincides with the intervals between the times

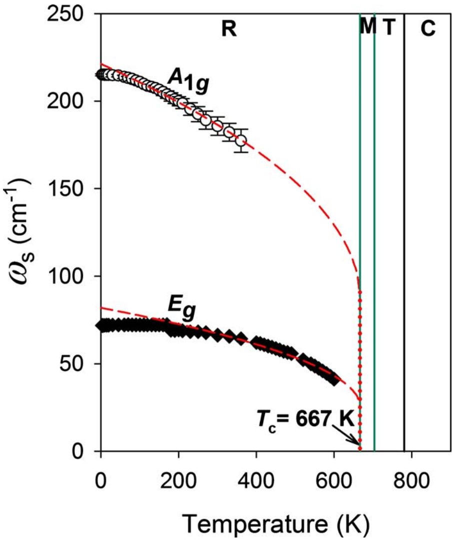

FIG. 7. (Color online) Temperature dependence of ω_s for the soft E_g and A_{1g} modes, where R, M, T, and C denote the rhombohedral, monoclinic, tetragonal and cubic phases. The dashed lines show the fittings to Eq. (4) that suggest the soft-mode driven first-order phase transition from R to M phase.

when the amplitude becomes zero for a DHO. Figure 7 plots the temperature dependence of ω_s for both E_g and A_{1g} modes. To further explore the soft-mode behavior quantitatively, the temperature dependence of ω_s for the soft modes was then fitted to

$$\omega_s = A(T_c - T)^{0.5} + \omega_{\text{offset}}. \tag{4}$$

The first term shows the usual temperature dependence of ω_s described by the framework of the Landau theory while the additional parameter, ω_{offset}, is introduced to take account the first-order nature of phase transition, as evidenced by the thermal hysteresis observed in DTA upon cooling and heating as well as the phase coexistence region suggested by XRD measurements.[7,20] In order to avoid the influences of the quantum-mechanical fluctuations as well as the mode anticrossing on ω_s, the fitting to Eq. (4) for the soft E_g mode was performed only with the results obtained at $T \geq 230$ K, at which mode b becomes almost vanished. By taking $T_c = T_{\text{R-M}} = 667$ K, which is consistent with that suggested by the previous DTA measurement,[7] the best fittings to Eq. (4) for the soft E_g and A_{1g} modes give $\omega_{\text{offset}} = 25.1$ and 86.4 cm^{-1}, and $A = 2.5$ and 8.2 for E_g mode and A_{1g} mode, respectively. The good fitting of experimental data to Eq. (4) suggests that the first-order phase transition from rhombohedral to monoclinic is purely soft-mode driven. Since the spectra obtained at $T > 600$ K are heavily overlapped and too broad for analyses, physical information about the monoclinic phase, which starts to appear only at ~650 K, could not be extracted in this study. Nevertheless, our micro-Raman measurements unveiled the soft-mode-driven first-order phase transition from rhombohedral to monoclinic phase.

IV. DISCUSSIONS

Having investigated the dielectric as well as the soft-mode behaviors, we revisit the controversial phase-transition sequence for AT based on our results. As mentioned previously, the change in $P_s \neq 0$ to $P_s = 0$ resulted by a ferroelectric to paraelectric phase transition should trigger a dielectric anomaly. Since no dielectric anomaly is observed for AT at 2.2 K $\leq T <$ 694 K, the occurrence of any ferroelectric phase transition within this temperature range is indeed very unlikely. Therefore, the previous argument on the phase transition associated with the ferroelectric phase with $R3c$ symmetry is not supported by our measurements. In contrast, the ground state with $R\bar{3}c$ symmetry is more consistent with the quantum paraelectricity as well as the XRD measurements in this study. Furthermore, the micro-Raman measurements suggest that the phase transition from rhombohedral to the higher-temperature monoclinic phase is soft-mode dominant, indicating that this transition involves only the rotations of oxygen octahedra.

On the other hand, the existence of extra Raman modes a–g seems to oppose the $R\bar{3}c$ symmetry ground state suggested by the dielectric measurements. This issue should be further addressed here. Since no dielectric anomaly was observed, the extra Raman modes should not correspond to a ferroelectric phase transition. By ruling out the possibility of ferroelectric phase transition, the extra modes a–g could be possibly brought about by either an occurrence of transition from an unreported paraelectric phase X to the higher temperature $R\bar{3}c$ phase, whereby a dielectric anomaly may not be induced; or the existence of symmetry-breaking regions (SBR) that act to relax the Raman selection rules. Since the extra peaks were observed at temperatures higher than RT, phase X should be reflected by our RT XRD measurements if the extra peaks are resulted from the macroscopic phase transition; however, our RT XRD trace for AT shows rhombohedral structure with $R\bar{3}c$ symmetry that is in good agreement with other reports.[10] Also, our XRD measurements performed down to 68.4 K show no profile change but only the downward shifts for diffraction peaks, suggesting the persistence of rhombohedral phase with $R\bar{3}c$ symmetry down to low temperatures. Therefore, the existence of paraelectric phase X is inconsistent with our experimental results. By justifying the unlikelihood of macroscopic phase transition from either ferroelectric or paraelectric to the higher temperature $R\bar{3}c$ phase, the extra peaks could be brought about by the existence of SBR. The existences of tan δ peaks, which are probably due to the defects or impurities, support the speculation of SBR, although their origins are currently unknown. When the local electric dipoles induced by the defects or impurities are involved in the dielectric medium, they could polarize the neighboring unit cells to form SBR, and it is plausible that the induced SBR grow simultaneously with increasing dielectric constant. Actually in AT, the extra peaks develop in accordance with the increase in dielectric constant upon cooling, implying the growth of SBR.

The next question that we have to discuss is the symmetry of SBR. Based on the aforementioned assumption, the symmetry of SBR should be polar, and possibly with $R3c$ symmetry. The consistency between the total number of observed modes at 3.5 K (12 Raman active modes) and that suggested by the factor-group analysis (13 active modes) for $R3c$ symmetry seems to support this physical picture. Furthermore, it is believed that the weak pyroelectricity of AT reported previously by Kugel *et al.*[6] may also be related to SBR. The relaxation of impurities can be described as hopping motions between two equal potential wells. Prior to the pyroelectric measurement, Kugel *et al.*[6] performed a prepoling with an external electric field (30 kV/cm) when cooling the sample from 200 to 70 K, the equal potential wells originally encountered by the relaxation of impurities becomes asymmetric (one of the well is deeper and the other one is shallower). The impurity dipoles are then aligned and the adjacent unit cells are polarized to form polar SBR. Upon cooling, these SBR may grow in size and induce a polar state, leading to the observed weak pyroelectricity.

V. CONCLUSIONS

In conclusion, AT ceramic has been synthesized by employing high-pressure oxygen sintering at $\sim$13 atm. Our micro-Raman measurements directly resolve the soft E_g and A_{1g} modes, which unveiled the soft-mode driven first-order rhombohedral to monoclinic phase transition. The absence of dielectric anomaly suggests that the previously proposed ferroelectric transition involving $R3c$ symmetry with $P_s \neq 0$ is very unlikely; however, the possibility of the existence of SBR with $R3c$ symmetry up to at least 360 K cannot be ruled out due to the observation of additional modes a–g. In overall, the physical picture with quantum paraelectric ground state that exhibits $R\bar{3}c$ symmetry with some embedded SBR is more consistent with our experimental results.

ACKNOWLEDGMENTS

This work was supported by both KAKENHI (Grant No. 20246098) and Global COE program, Education and Research Center for Material Innovation-Program for Upbring International Leaders on Future Materials.

---

*itoh.m.aa@m.titech.ac.jp

[1] H. Kato, H. Kobayashi, and A. Kudo, J. Phys. Chem. B **106**, 12441 (2002).
[2] M. Valant, A. Axelsson, and N. Alford, J. Eur. Ceram. Soc. **27**, 2549 (2007).
[3] D. Fu, M. Endo, H. Taniguchi, T. Taniyama, and M. Itoh, Appl. Phys. Lett. **90**, 252907 (2007).
[4] H. T. Kim, T. Shrout, C. Randall, and M. Lanagan, J. Am. Ceram. Soc. **85**, 2738 (2002).
[5] M. B. Telli, S. S. N. Bharadwaja, M. D. Biegalski, and S. Trolier-McKinstry, Appl. Phys. Lett. **89**, 252907 (2006).
[6] G. E. Kugel, M. D. Fontana, M. Hafid, K. Roleder, A. Kania, and M. Pawelczyk, J. Phys. C **20**, 1217 (1987).
[7] A. Kania and A. Ratuszna, Phase Transitions **2**, 7 (1981).
[8] A. M. Glazer, Acta Crystallogr., Sect. B: Struct. Crystallogr. Cryst. Chem. **28**, 3384 (1972); Acta Crystallogr., Sect. A: Cryst. Phys., Diffr., Theor. Gen. Crystallogr. **31**, 756 (1975).
[9] G. A. Komadin, A. A. Volkov, V. V. Voĭtsekhovskĭ, J. Petzelt, and A. Kania, Phys. Solid State **37**, 1444 (1995).
[10] M. Wołcyrz and M. Łukaszewski, Z. Kristallogr. **177**, 53 (1986).
[11] W. R. Abel, Phys. Rev. B **4**, 2696 (1971).
[12] G. Rupprecht and R. O. Bell, Phys. Rev. **135**, A748 (1964).
[13] J. H. Barrett, Phys. Rev. **86**, 118 (1952).
[14] K. A. Müller and H. Burkard, Phys. Rev. B **19**, 3593 (1979).
[15] Y. Inaguma, J. H. Sohn, I. S. Kim, M. Itoh, and T. Nakamura, J. Phys. Soc. Jpn. **61**, 3831 (1992).
[16] R. Wang and M. Itoh, Ferroelectrics **262**, 125 (2001).
[17] E. K. H. Salje, B. Wruck, and H. Thomas, Z. Phys. B **82**, 399 (1991).
[18] J. Petzelt, S. Kamba, E. Buixaderas, V. Bovtun, Z. Zikmund, A. Kania, V. Koukal, J. Pokorny, J. Polivka, V. Pashkov, G. Komandin, and A. Volkov, Ferroelectrics **223**, 235 (1999).
[19] J. F. Scott, Phys. Rev. **183**, 823 (1969).
[20] M. Pawełczyk, Phase Transitions **8**, 273 (1987).